ARTICLE

High Resolution Characterization of Engineered Nanomaterial Dispersions in Complex Media Using Tunable Resistive Pulse Sensing Technology

Anoop K. Pal,[†,*] Iraj Aalaei,[†] Suresh Gadde,[∥] Peter Gaines,[¥] Daniel Schmidt,[§,⊥] Philip Demokritou,[#] and Dhimiter Bello[‡,⊥,#,*]

[†]Biomedical Engineering and Biotechnology Program; [‡]Department of Work Environment, College of Health Sciences, [¥]Department of Biological Sciences, [§]Department of Plastics Engineering; [⊥]Center for High-Rate Nanomanufacturing, University of Massachusetts Lowell, Lowell, Massachusetts 01854, United States, [∥]Brigham and Women's Hospital, 45 Francis Street, Boston, Massachusetts 02115, United States, and [#]Center for Nanotechnology and Nanotoxicology, Department of Environmental Health, Harvard School of Public Health, 677 Huntington Avenue, Boston, Massachusetts 02115, United States

ABSTRACT *In vitro* toxicity assessment of engineered nanomaterials (ENM), the most common testing platform for ENM, requires prior ENM dispersion, stabilization, and characterization in cell culture media. Dispersion inefficiencies and active aggregation of particles often result in polydisperse and multimodal particle size distributions. Accurate characterization of important properties of such polydisperse distributions (size distribution, effective density, charge, mobility, aggregation kinetics, *etc.*) is critical for understanding differences in the effective dose delivered to cells as a function of time and dispersion conditions, as well as for nano–bio interactions. Here we have investigated the utility of tunable nanopore resistive pulse sensing (TRPS) technology for characterization of four industry relevant ENMs (oxidized single-walled carbon nanohorns, carbon black, cerium oxide and nickel nanoparticles) in cell culture media containing serum. Harvard dispersion and dosimetry platform was used for preparing ENM dispersions and estimating delivered dose to cells based on dispersion characterization input from dynamic light scattering (DLS) and TRPS. The slopes of cell death *vs* administered and delivered ENM dose were then derived and compared. We investigated the impact of serum protein content, ENM concentration, and cell medium on the size distributions. The TRPS technology offers higher resolution and sensitivity compared to DLS and unique insights into ENM size distribution and concentration, as well as particle behavior and morphology in complex media. The *in vitro* dose–response slopes changed significantly for certain nanomaterials when delivered dose to cells was taken into consideration, highlighting the importance of accurate dispersion and dosimetry in *in vitro* nanotoxicology.

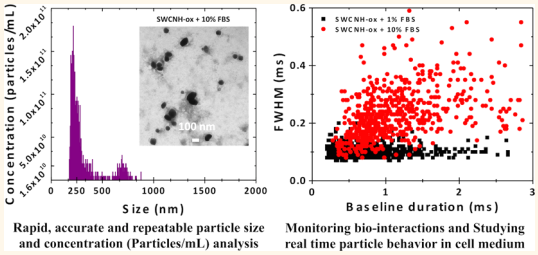

KEYWORDS: nanomaterial · size distribution · TRPS · DLS · effective density · cytotoxicity

Precise characterization of key properties of engineered nanomaterial (ENM) dispersions in cell culture media, in particular of size distribution, agglomeration state, effective density of formed agglomerates, shape, and protein corona effects, are crucial for understanding nanomaterial toxicity, as well as for linking ENM physiochemical properties with their biological activity, immune interactions and toxicity.[1−6] Adequate characterization of the distribution of key ENM properties such as hydrodynamic size distribution, number concentration, charge, and protein corona in the wet state, as delivered to the cells and as a function of time, is of paramount importance in nanotoxicology and nanomedicine applications.

To achieve improved dispersion of nanomaterials for biological testing, different dispersion protocols are applied that involve various dispersion media, surfactants, sonication energies, and other experimental parameters[7,8] that can alter the properties of the resultant dispersions and the (nano)particles they contain.[9,10] Reproducibility of dispersions across different experiments and between different protocols may vary, and the magnitude of the effects of such variations in dispersion (and hence dose) variations on toxicological and other outcomes of interest often goes unrecognized.

* Address correspondence to dhimiter_bello@uml.edu, pal.k.anoop@gmail.com.

Received for review April 22, 2014 and accepted August 5, 2014.

Published online August 05, 2014
10.1021/nn502219q

However, such effects can be significant.[8,11] Developing reproducible, generalizable and well-defined dispersion protocols for *in vitro* toxicity assessment, coupled with dosimetry models that can predict reasonably accurately the delivered and effective dose to cells is critically important to *in vitro* nanotoxicology and nanomedicine.[12−14] Investigation of other phenomena, such as the kinetics of particle−particle and particle−biomolecule interactions in liquid medium, is also of great interest.[15,16]

Key nanomaterial characterization parameters for nano−bio interactions, especially in *in vitro* toxicity evaluations and nanoparticle−cell interactions include size distribution, dispersion stability, effective density of agglomerates, shape, and chemical composition.[17−19] The vast majority of *in vitro* testing platforms use cell culture media containing between 1 and 10% of serum (such as fetal bovine serum, FBS), which may alter any and all of these properties.[1,20,21] Furthermore, characterization of ENM dispersions must be performed under biologically relevant conditions using realistic doses, at much lower ENM concentrations (0.1−10 μg/mL) than those used in the past.[22,23] Therefore, nanoparticle characterization techniques should be able to accurately measure polydisperse distributions in complex cell culture media at or below 1−10 μg/mL ENM concentrations.

Several techniques, including dynamic light scattering (DLS), transmission electron microscopy (TEM), scanning electron microscopy (SEM), atomic force microscopy (AFM), and ultracentrifugation have been used for characterizing nanomaterial dispersions.[24−28] Microscopy techniques typically measure the size in the dry state rather than the dispersed state, and different artifacts may be introduced during sample preparation. In a recent study, DLS, TEM, and AFM were used to analyze a colloidal gold dispersion and all three techniques measured the same nominal size. When the particles were incubated with human plasma, however, the TEM and AFM measurements gave the same nominal sizes as in phosphate-buffered saline (PBS), whereas the DLS reported size almost doubled.[29] Such changes in the size and charge of a particle are important because they could alter the biodistribution, toxicity, or immunological profile of the nanomaterial. Therefore, it is highly advisible to use at least two complementary analytical techniques for characterizing ENM dispersions.[30,31]

DLS and similar techniques that rely on light scattering principles measure size and charge based on the average mobility of the particles in solution. DLS is currently the preferred technique for nanomaterials dispersion characterization due to its ease of use, high level of automation, high throughput nature, and its applicability to a broad range of particle types and dispersion media. DLS is capable of analyzing a variety of nanomaterials in different media, but DLS results are limited by an inherent bias toward the largest particles present[32,33] and is not suitable for size analysis of highly polydisperse systems.[34] DLS systems measure directly intensity weighed size distributions. Such size distributions can be converted to the more appropriate for most nano−bio studies number or volume weighed size distributions but only under the assumption of spherical particles and a specific absorbance values.[35] Those assumptions can introduce a significant bias into the measurements and result to significant deviations and might be even biased toward the smaller population, if conducted in media containing serum proteins. These measurements become more unreliable if ENM dispersions are further diluted in protein-containing medium, because the nanoparticle/protein content ratio varies, causing remodeling of the protein corona thickness on nanoparticles as well as the surface charge and skewing the size distributions as a result. In addition, DLS is unable to provide information concerning particle shape, and instead returns the hydrodynamic radius of the equivalent spherical particle. The relationship between this value and the actual dimensions of nonspherical particles is, therefore, crude at best. These issues are all the more important in the case of dispersions involving serum proteins (FBS), routinely used in cellular studies.

Here we have explored the utility of nanopore based tunable resistive pulse sensing (TRPS) technology and optimized its use for characterization of ENM dispersions in realistic, complex cell culture media containing serum, conditions applicable to *in vitro* nanotoxicology and nanomedicine studies. TRPS, which is based on the Coulter principle, has been used recently for size and concentration analysis of particles from the micrometer range to the nanoscale (with a lower detection size limit of ~40 nm), as well as to infer information about key properties in solution, including their charge,[36−38] shape,[39−41] and conductivity.[42] The TRPS technology does not rely on light scattering properties of ENMs. Instead, it monitors changes in ionic current as individual nanoparticles (or agglomerates) pass through an elastomeric membrane containing a single (nano)pore whose size is precisely controlled.[33,34,43] The TRPS monitors particles one-by-one and provides population statistics based on thousands of individual measurements.

Accurate characterization of ENM size distributions in nanotoxicology and nanomedicine is a worthy pursuit on its own, and it is becoming more so in the context of numerical modeling such as ISDD (*in vitro* sedimentation, diffusion and dosimetry model), which are utilized to estimate delivered dose to cells over time. One important input parameter in these models is the average hydrodynamic diameter ($d_{h,z\text{-}ave}$) of agglomerates. In addition, the effective density and size of formed agglomerates in culture media plays

TABLE 1. Summary Description of the Engineered Nanomaterials Tested in This Study

nanomaterial label	description	source [ref]	primary particle size from vendor (nm)	surface area ($m^2\ g^{-1}$)	material bulk density (g/cm^3)	effective density[a] (g/cm^3)	DSE_{cr}[b] (J/mL)
SWCNH-ox	single wall carbon nanohorns, H_2O_2 oxidized	Donated by NEC Co., Japan [48, 49]	OD = 1−2; Aggl. = 50−100	1154	1.25	1.25	161
Printex-90	carbon black	Degussa [50, 51]	14	236	1.85	1.24	262
CeO_2	cerium oxide	UC Center for Environmental Implications of Nanotechnology [52]	7−25	87	7.65	1.69	262
Ni Inco	nickel nanoparticles	Inco specialty powders; Donated from Prof. A. Elder, U Rochester	60 ± 10	91	8.19	1.78	262

[a] Density of agglomerates in dispersion medium (RPMI +10% FBS) determined according to DeLoid *et al.* (2014). [b] DSE_{cr}, Critical dispersion energy.

TABLE 2. Characterization of Four Engineered Nanomaterial (ENM) Dispersions (at 50 μg/mL) in RPMI with 10% FBS Cell Culture Medium Obtained from Dynamic Light Scattering[a] and Tunable Resistive Pulse Sensing

	dynamic light scattering (DLS)				tunable resistive pulse sensing (TRPS)				
ENM type	$d_{h,z\text{-ave}}$ (nm)	PdI	ζ (mV)	peak size	size mean (nm)	size mode (nm)	range (nm)	concentration[b] (#/mL)	fraction of total number
SWCNH-ox	261 ± 3	0.23	−9.3 ± 1.0	small	249	212	177−572	2.70×10^{10}	0.844
				large	660	684	572−877	5.00×10^{09}	0.156
Printex- 90	270 ± 8	0.37	−13.1 ± 1.1	small	264	198	173−717	9.80×10^{07}	0.971
				large	1068	860	717−1476	2.90×10^{06}	0.029
CeO_2	265 ± 2	0.31	−12.1 ± 0.2	small	268	211	183−659	1.80×10^{08}	0.987
				large	1066	847	659−1922	2.60×10^{06}	0.013
Ni Inco	234 ± 7	0.40	−14.4 ± 1.5	small	268	199	176−715	8.80×10^{07}	0.990
				large	1136	904	715−1897	4.10×10^{06}	0.010

[a] $d_{h,z\text{-ave}}$, hydrodynamic diameter; PdI, polydispersity index, a measure of the broadness of size distribution; ζ, Zeta Potential, a measure of surface charge in the cell culture medium. [b] Concentration for SWCNH-ox determined at 5 μg/mL.

important roles in determining particle mobility in suspension and thus affect the overall ENM dose delivered to the cells *in vitro*, with larger agglomerates settling faster than smaller ones and potentially impacting dose during earlier time points. The question of whether such differences in size distributions measured by different techniques or over time impact toxicological outcomes is an important one, which we have addressed in this work. We demonstrate here that the TRPS technology offers unique advantages over DLS for ENM size distribution and concentration analysis and for studying particle behavior in cell culture media, including excellent sensitivity, and high resolution. Furthermore, we investigated changes in the slopes of cell death as a function of administered and delivered doses using size distribution inputs from DLS and TRPS and show that the most notable changes in dose−response slopes result from the use of delivered dose instead of the administered one, and less so from differences in the measured size distribution by DLS and TRPS.

RESULTS AND DISCUSSION

TRPS *vs* DLS for Characterization of Nanoparticle Dispersions. A previously reported, optimized, and standardized ENM dispersion protocol was used for dispersion of four representative ENMs (Table 1) in cell culture medium with 10% FBS.[11,30] Results including hydrodynamic diameter ($d_{h,z\text{-ave}}$), polydispersity index (PdI) and charge are summarized in Table 2. DLS measured hydrodynamic sizes ($d_{h,z\text{-ave}}$) for all four ENMs were in the 230−270 nm range, with polydispersity values varying between 0.23 and 0.4, representing relatively monodisperse size distributions. Ni Inco had the highest PdI values (0.4), whereas SWCHN-ox had the lowest PdI (0.23). These DLS values are similar to those reported previously.[44−46] Higher PdI values are driven by greater agglomeration/aggregation of particles in the ENM dispersions (typical for Printex 90 and Ni Inco), verified by time-series DLS measurements (data omitted). It should be noted that Ni Inco in particular and Printex 90 to a lesser extent are difficult materials to disperse efficiently and stabilize.[45,47] Dispersions based on our protocol are reproducible and notably stable over 24 h duration (data not shown).

Figure 1 compares DLS size distributions (intensity, %) to that of TRPS (concentration, particles/mL) measured side-by-side for the same ENM dispersions at 50 μg/mL mass concentration. Note that TRPS size distribution measurements are bimodal, with a primary mode very close to the DLS peak (peak maxima 250−270 nm), and a secondary mode with a maximum in the 700−900 nm range and a tail extending beyond 2 μm. The TRPS modes are much sharper (narrower) compared to DLS and in two occasions fully resolved. Since dispersions were prepared in medium

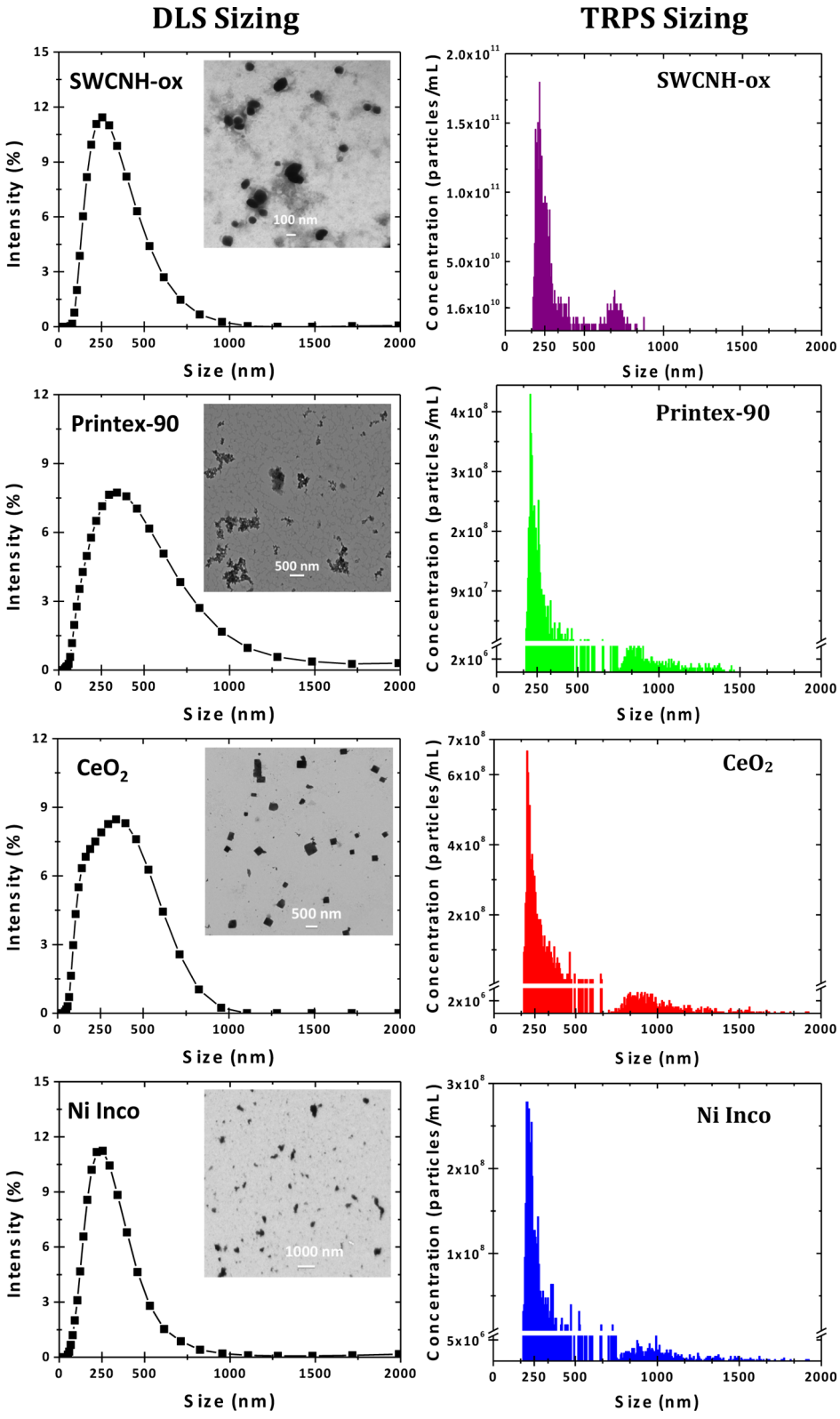

Figure 1. Comparisons of ENM size distributions as determined by dynamic light scattering (DLS, left panel), tunable resistive pulse sensing (TRPS, right panel), and transmission electron microscopy (TEM, inserts). A secondary peak related to agglomerates of primary particles centered around 700−1000 nm is fully resolved in TRPS but absent in DLS. Note also that DLS size distributions are much broader than TRPS size distributions.

containing FBS, the DLS measured size distributions are influenced by the high content of serum proteins, which can be seen in the small particle tail of the size distributions (<50 nm) in Figure 2.

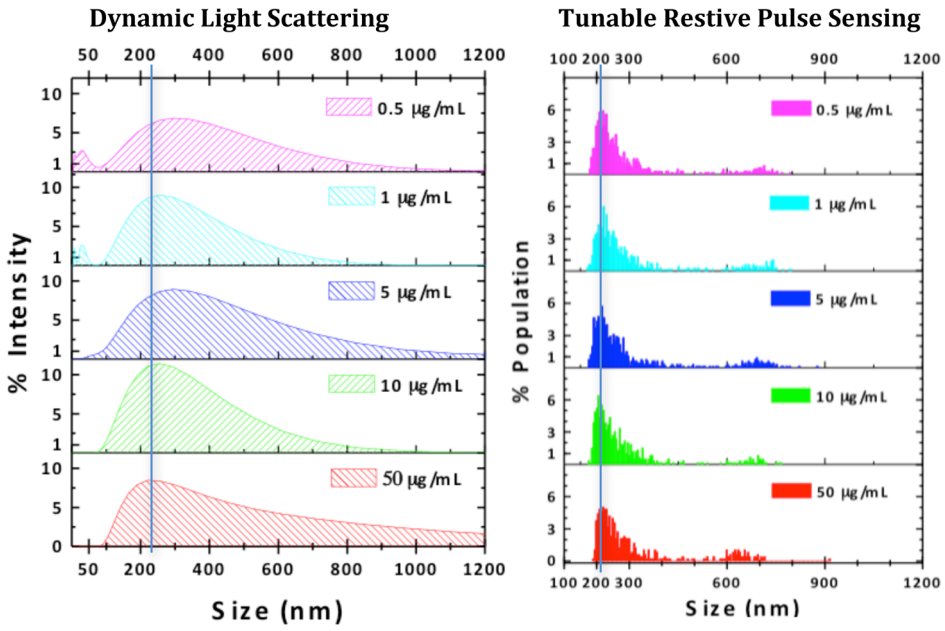

Figure 2. Comparative evaluation of TRPS and DLS in characterizing sensitivity and stability of size distribution measurements of a series of sequential dilutions of SWCNH-ox in the range of 0.5−50 μg/mL, prepared from a stock solution of 500 μg/mL in RPMI+10% FBS. The graphs represent averages of triplicate measurements. Note changes in the DLS size distributions below 5 μg/mL, especially left-side broadening of the peak and appearance of a smaller peak <50 nm, related to proteins in serum. At higher concentrations (50 μg/mL) the peak broadened to the right, In contrast to DLS, the TRPS size distribution remained fairly constant over the whole concentration range.

Direct measurements of alternative dose metrics in liquid cell culture media/other realistic complex biological systems, especially number concentration, is highly desirable. Because TRPS counts each particle individually and simultaneously collects information on its size, and (to some extent) particle shape, TRPS is capable of measuring particle number concentration in dispersions (in particles/mL). As summarized in Table 2, TRPS number concentration measurements for the standard concentration of 50 μg/mL reveal that the particle concentrations associated with the second mode of the distributions (larger agglomerates) constituted 1.0, 1.3, and 2.9% of the total particle number concentration for Ni Inco, CeO_2 and Printex 90 samples, respectively, *i.e.*, about 2 orders of magnitude fewer particles by number than those in the nano size range. However, for SWCNH-ox, the second mode of the distribution constituted 15.6% of the total particle number concentration, representing a substantial subpopulation of agglomerates. In terms of absolute number concentration at the same mass concentration of 50 μg/mL, the highest number concentration was recorded for SWCNH-ox (3.2×10^{10} particles/mL), whereas the lowest was measured for Ni Inco (9.21×10^{7} particles/mL). TEM images (inserts in Figure 1) are qualitatively in agreement with direct measurements, especially TRPS data, in that the presence of distinct subpopulations of larger agglomerates are clearly visible in the midst of otherwise well-dispersed ENMs with primary sizes in the 200−300 nm range.

Because of the differences in size distributions between the two techniques (single size distribution in DLS *vs* bimodal distribution in TRPS, Figure 1), the DLS size distributions are compared to the corresponding primary TRPS (peak) size distributions. The second peak in TRPS is analyzed separately. In DLS, the width of the particle size distribution is measured by the PdI index. In TRPS, because the data were right skewed (and fitted a log-normal distribution), we calculated separately for each peaks summary statistics common for log-normal distributions (geometric mean and geometric standard deviation, GSD). As can be seen from Table 2, the arithmetic mean of DLS and the TRPS (peak 1) size distributions compare reasonably well. The relative difference in the average agglomerate size was in the range of 0.8% (CeO_2) to 14.5% (for Ni Inco), with DLS resulting in slightly larger average sizes in 2 out of 4 cases. The mode for TRPS peak 1 was notably smaller than DLS mean values. The GSD of peak 1 was 1.2−1.4 for all materials. The range (min-max) of particle sizes for TRPS peak one varied as follows: SWCNH-ox (177−572 nm), Printex (173- 717 nm), Ni Inco (176−715 nm), and CeO_2 (183−659). The GSD for peak 2 was 1.1 (SWCNH-ox) to 1.3 (Ni Inco), with the maximum size range varying from 877 nm (SWCNH-ox) to 1.9 μm for CeO_2 and Ni.

The surface charge (zeta potential) as measured by DLS in cell culture media ranged from -9.3 ± 1.0 to -14.4 ± 1.5 mV, typical for the cell culture medium (Table 2). In contrast, surface charge in DI water was different, with Ni Inco, CeO_2 and Printex 90 showing

TABLE 3. Effect of Sequential Dilution of a 500 μg/mL SWCNH-ox Stock Dispersion in RPMI +10% FBS Cell Culture Medium on Hydrodynamic Size and Charge Obtained from Both Dynamic Light Scattering and Tunable Resistive Pulse Sensing

		dynamic light scattering (DLS)			tunable resistive pulse sensing (TRPS)		
SWCNH-ox (500 μg/mL) dilution in RPMI+10% FBS	expected SWCNH-ox concentration (μg/mL)	$d_{h,z\text{-ave}}$ (nm)	PdI	ζ (mV)	size mean (nm)	size mode (nm)	concentration (#/mL)
1:10	50	311 ± 11	0.37	−9.3 ± 1.0	317	228	—[a]
1:50	10	223 ± 1	0.28	−7.3 ± 0.3	291	204	—[a]
1:100	5	240 ± 4	0.48	−7.6 ± 1.0	315	210	3.2×10^{010}
1:500	1	70 ± 2	1	−7.6 ± 0.9	313	223	6.9×10^{009}
1:1000	0.5	43 ± 2	1	−8.0 ± 0.7	297	208	5.7×10^{008}

[a] Concentration was too high, resulting in pore clogging. The applied pressure had to be reduced to near 0 (0 for 1:10 and 0.5 Pa for 1:50), which results in unreliable measurements. Stock dilution was necessary.

positive charges (not shown). It is now well-known that in cell culture medium, the surface charge of different nanoparticles converges to that of the media itself because of the protein corona effect.[11] For this reason, comparison of surface charge size distributions between DLS and TRPS in cell culture medium would be of lesser interest than distributions of surface charge in DI water and should be pursued in future work.

Sensitivity. The sensitivities of the DLS and TRPS techniques for size distribution measurements were investigated in detail with a series of sequential dilutions of SWCHN-ox dispersions over the 0.5−50 μg/mL concentration range in RPMI+10% FBS. This *in vitro* nanoparticle concentration range reflects better realistic human nanoparticle exposures. Given the general trend in *in vitro* nanotoxicology to use lower nanoparticle concentrations, including below 1 μg/mL, direct measurements of number concentration and other dispersion parameters at very low doses have become more critical, and are essential for air-to-liquid delivery systems, where delivered ENM dose is unknown. The comparative data on size distributions as measured by DLS and TRPS is summarized in Figure 2 and Table 3. Note that DLS measurements produced very broad unimodal size distributions across all concentrations. The measured $d_{h,z\text{-ave}}$ decreased from 311 nm (at 50 μg/mL) to 43 nm (at 0.5 μg/mL), this later peak corresponding to serum proteins (confirmed with blanks). In addition, the PdI increased from 0.3 to 0.4 to 1 below 1 μg/mL.

In contrast, TRPS size distributions remained bimodal (maxima at ~220 and 660 nm) and with well-resolved modes which did not change notably as a function of concentrations down to 0.5 μg/mL. More careful analysis of the TRPS size distribution data as a function of concentration indicated a modest decrease in size at lower ENM concentration (Table 3), which might be due to better ENM stabilization at higher serum/particle ratios. A slight shift in the maxima of peak 2, second mode (650−700 nm) is also noted. The rate of particles going through the pore also dropped from 1000 particles/min (at 50 μg/mL) to 134 particles/min (at 0.5 μg/mL), consistent with the presence of fewer particles in suspension.

TRPS has a lower cut-point of 40 nm and serum proteins are not measured. Nanoparticle agglomerates and aggregates acquire protein corona and stable dispersions below 100 nm are rarely achieved. In addition, we could not find experimental evidence from TEM imaging and the lower end of the TRPS size distribution for particle agglomerates less than 50 nm. This limitation should be kept in mind and this is another reason why two nanoparticle characterization techniques are desirable. Recently, Anderson *et al.* (2013) showed that TRPS is better suited for determining actual size distributions for particles that are not monomodal, consistent with our observations for polydisperse size distributions of nanomaterials dispersed in serum containing cell culture medium (Table 3).

Impact of Size Distribution Differences on Toxicological Outcomes. The ENM dose delivered to cells for all ENMs was estimated using the recently developed Integrated Dosimetry platform at the Harvard Center for Nanotechnology and Nanotoxicology[12−14] which combines measurements of effective density of formed agglomerates as described by DeLoid *et al.*[12] followed by numerical calculation of the cell deposited dose as a function of time. Both DLS and TRPS determined hydrodynamic sizes were used for all ENM dispersions. Delivered doses to cell were estimated using the TRPS determined hydrodynamic sizes ($d_{h,z\text{-ave}}$) separately for each of the two modes from smaller and larger peak sizes. The estimated deposited dose fraction $f_D(t)$ function of each mode of the TRPS size distribution data was material and size dependent (Figure 3). The deposited dose estimates of the larger agglomerates (red line) of carbonaceous ENM, namely SWCNH-ox and Printex 90, were much lower than the corresponding doses of the metal oxide (CeO_2) and the Ni Inco ENMs, especially at earlier time points. For example, at 6 h, only 12% of SWCNH-ox and 20% of Printex 90 were estimated to deposit, compared to 100% of this larger

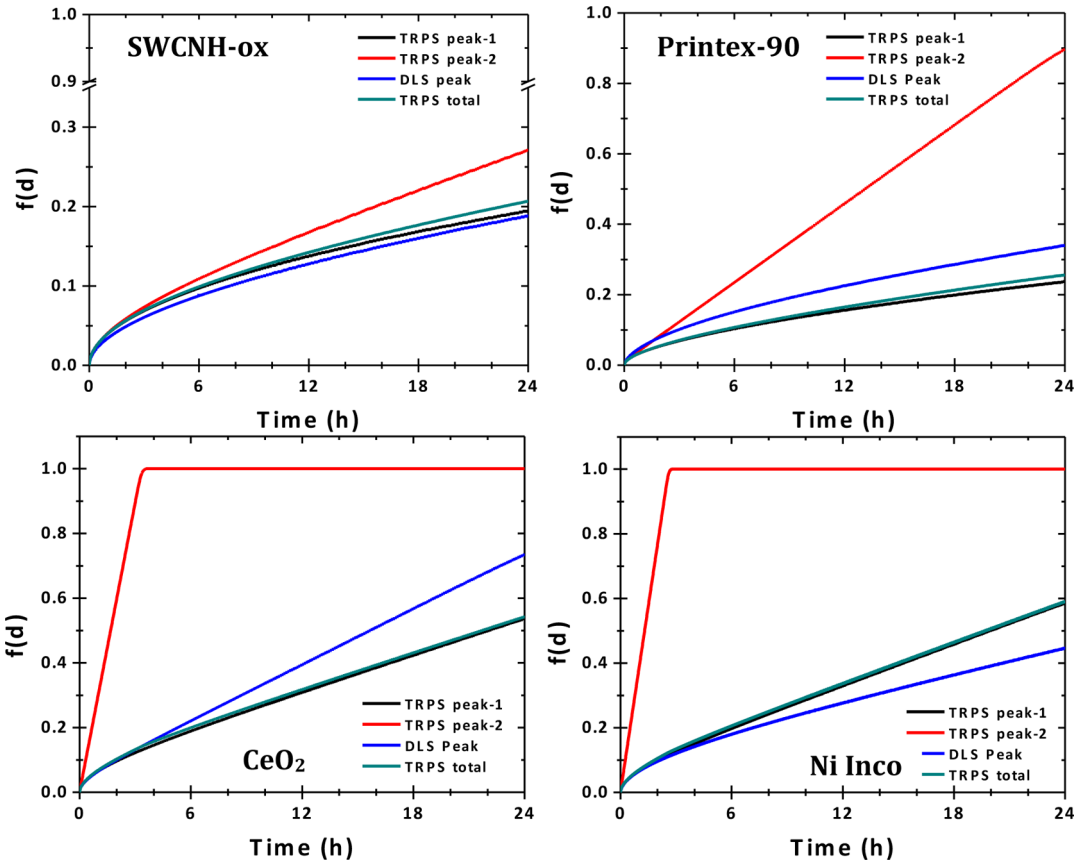

Figure 3. ISDD-model estimates of the deposited dose fraction $f_D(t)$ over 24 h for all ENMs. Hydrodynamic particle size in cell culture medium (Table 2) and the effective density of agglomerates (Table 1) were used as input in the dose model. The TRPS delivered dose estimate takes into account relative contribution of both peaks as detailed in the methods section (TRPS peak-1, maxima 200−250 nm range; TRPS peak-2, larger agglomerates peak with maxima in the 650−1200 nm). For peak 2, the effective density was assumed to be equal to that of peak 1. Given that effective density of peak 2 can only be smaller than or equal to the effective density of peak 1, this conservative estimation will result in smaller deposited fraction for the two carbonaceous ENM (SWCNH-ox and Printex-90), but it will not have any impact on CeO_2 and Ni Inco, both of which reach 100% deposition in under 3 h.

size fraction for CeO_2 and Ni Inco, both of which are expected to deposit completely within ~3 h.[13,14] Less than 30% of the larger SWCNH-ox, agglomerates (by number) were estimated to deposit at 24 h. For Printex 90, with the larger size mode at 1067 nm and 3% of the total particle number population, Table 2, 85% of this fraction (by number) was estimated to deposit at 24 h. For CeO_2 and Ni Inco, the deposited doses at 24 h were estimated to be 55 and 60%, respectively. The net $f_D(t)$ function (green line), however, seems to be driven primarily by the larger concentration of the smaller aggregate size, as seen in Figure 3. Figure 3 also highlights an important point that toxicity at earlier time points (2−6 h) in cellular studies may be influenced disproportionately by the initially high deposited doses (in terms of mass if not number) of large agglomerates, after which increasing local concentrations of smaller particles drive subsequent effects. For Printex 90 and CeO_2, the deposited fraction $f_D(t)$ TRPS peak 1 (black line) was smaller than DLS (blue line), for SWCNH-ox it was equal to DLS, whereas for CeO_2 it was larger than DLS. Contribution of peak 2 to the overall dose was also material dependent. For SWCNH-ox, the larger size peak (15.6% of the total particle population) contributed additionally to the deposited dose beyond that provided by peak 1 at 6 and 24 h, resulting in a slightly higher total deposited dose fraction by TRPS. Similarly, for Ni Inco, the TRPS-based deposited dose was higher than that based on DLS. The TRPS calculated overall deposited dose fraction $f_D(t)$ for CeO_2 and Printex 90 was smaller than the DLS fraction (Table 4).

Although we did not measure the delivered dose to cells for these materials in the present study, independent model validation was recently conducted for over 20 metal oxides using neutron activation and gamma ray real-time monitoring, including the CeO_2. The model predicted deposition dose was within 5% of the measured values.[14]

These differences in deposited dose fractions for the two different modes observed in the TRPS size distributions may have implications for cellular toxicity outcomes, especially when comparative toxicity evaluations of ENMs are performed. The question is, how significant is the impact?

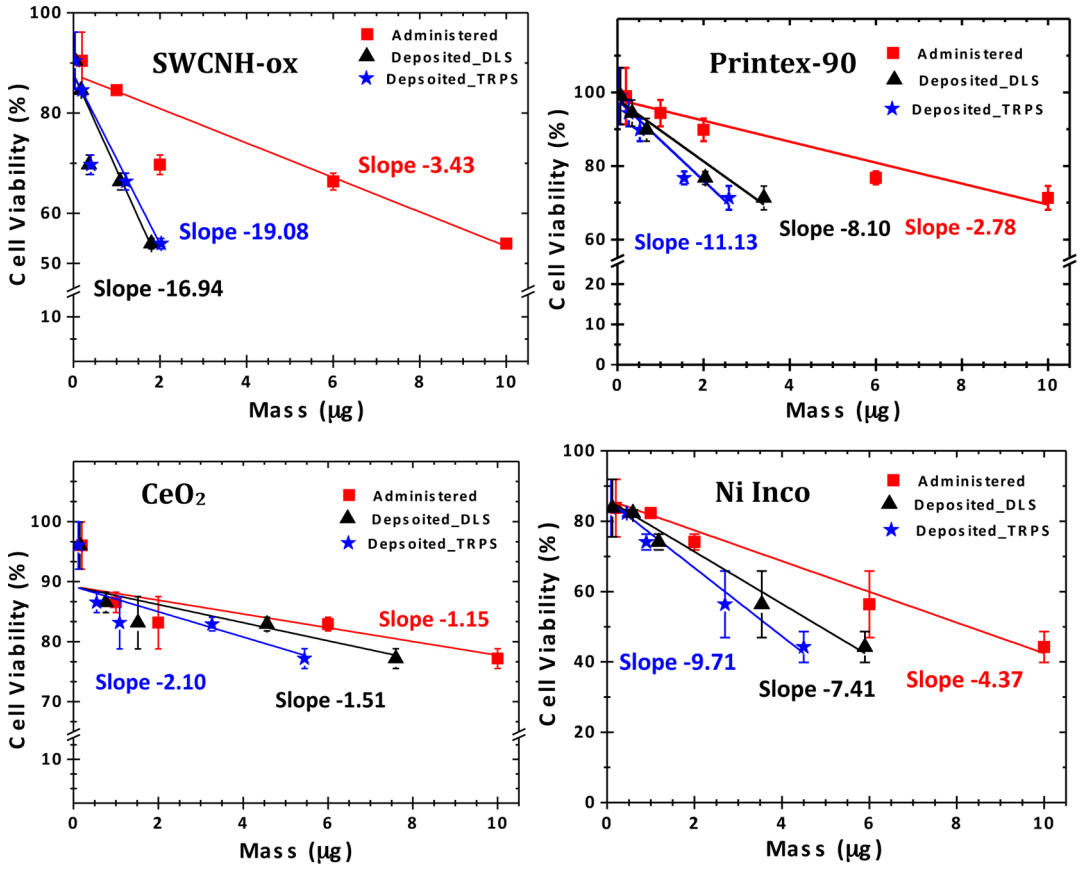

Figure 4. Slopes of cell viability and derivation of IC50 (mass dose causing 50% cell death) for test ENM as a function administered and deposited doses, using DLS and TRPS size distributions as model input parameters. Notable changes in the slopes of cell viability *vs* mass dose occur when deposited doses are taken into account. Better characterization of size distributions further alters the dose–response slopes. The magnitude of these effects is ENM dependent and relatively small compared to administered dose.

TABLE 4. Assessing the Impact of Deposited Dose on the Cell Viability–Mass Dose Response *In Vitro* for Four Test Nanoparticles[a,b,c]

characterization technique		dynamic light scattering (DLS)			tunable resistive pulse sensing (TRPS)				
nanomaterial label	time (h)	*f*(*d*)	MTT slope	IC50 (μg)	*f*(*d*)	MTT slope	IC50 (μg)	% $\Delta f(d)$	DLS/TRPS MTT slope ratio
SWCNH-ox	6	0.09	−16.83	2.56	0.10	−18.70	2.30	−11.11	0.90
	24	0.19	−16.94	2.11	0.20	−19.08	1.87	−5.26	0.89
Printex-90	6	0.16	−8.53	5.07	0.11	−12.41	3.49	31.25	0.69
	24	0.34	−8.10	5.80	0.26	−11.13	4.22	23.53	0.73
CeO_2	6	0.24	−7.81	6.15	0.21	−7.45	6.45	12.50	1.05
	24	0.74	−1.51	26.83	0.54	−2.10	19.29	27.03	0.72
Ni Inco	6	0.19	−3.95	8.92	0.21	−3.40	10.36	−10.53	1.16
	24	0.45	−7.41	4.61	0.59	−9.71	3.52	−31.11	0.76

[a] Legend: *f*(*d*), deposited dose fraction; MTT, cell viability assay; IC50, ENM dose (μg) inducing 50% cell death; Calculated as % $\Delta f(d) = 100 \times [[f(d)_{DLS} - f(d)_{TRPS}]/f(d)_{DLS}]$. [b] Effective density of the larger agglomerates (TRPS peak 2) was unknown and assumed to be equal to that of smaller agglomerates presented in Table 1. Since large agglomerates likely trap more liquid media inside relative to smaller agglomerates, their effective density may be slightly lower. Hence, the $f_D(t)$ estimates for large agglomerates may be slightly overestimates. Sensitivity analysis using smaller effective densities suggests this is a negligible effect. [c] Deposited dose fraction was estimated based on size input obtained form dynamic light scattering (DLS) and tunable resistive pulse sensing (TRPS) in the ISDD model at two time points, 6 and 24 h. The ratio of slopes provides a quick indicator of the magnitude of differences in the outcome of interest (slope of dose–response). Note that for carbonaceous ENM, this ratio is within ~10% of 1.0, and independent of time. For the metal/metal oxide category, the smaller peak of large agglomerates impacts the early time pints (ratio 1.05–1.16), whereas for later time points, this ratio drops to 0.72–0.75, suggesting higher delivered dose estimated based on DLS input relative to TRPS.

Cell viability as a function of administered and model estimated deposited dose for the four test ENM is plotted in Figure 4. The dose–response slopes become much steeper for the deposited dose based on DLS size distribution measurements, compared to administered doses and reflect material-specific

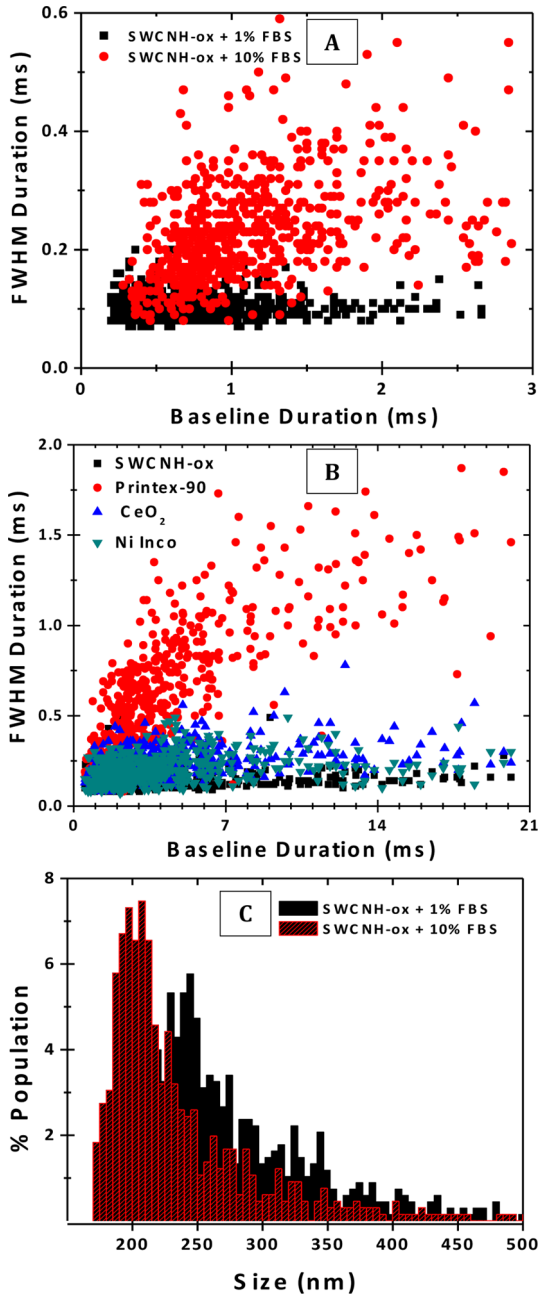

Figure 5. Relationship between baseline duration *vs* full width at half-maximum (fwhm) values, used for assessing ENM particle behavior in cell culture media. (A) SWCNH-ox in 1 and 10% FBS. (B) Four representative ENM under conditions of standardized dispersion protocol. (C) Changes in size distribution for SWCNH-ox stabilized with different amounts of protein, 1 and 10% FBS, respectively.

deposited fraction data $f_D(t)$, in Figure 3. The cell viability slopes for Carbon based ENMs were significantly steeper for the deposited doses based on DLS-data than the administered mass doses. SWCHN-ox had the maximum negative slope followed by Printex-90, Ni Inco and CeO_2 (Table 4). The TRPS-derived effective dose was calculated as described in the Materials and Methods section taking into consideration deposition fraction (Figure 3) of each peak and their relative abundance (Table 2). The TRPS delivered dose varied somewhat from the DLS dose, leading to differences in respective slopes (Table 4). The ratio of DLS/TRPS delivered dose slopes varied from 0.9 for SWCNH-ox (*i.e.*, 10% discrepancy) to 0.76 for Ni Inco (*i.e.*, 24% discrepancy). The overall trend of these calculations is that better characterization of size distributions in dispersions results in slightly stronger dose–response slopes. For the tested materials, the magnitude of this effect varied from 10 to 30%, with larger discrepancies seen for denser ENM. Nevertheless, the highest impact in the dose–response slopes results from consideration of the delivered dose to cells (Table 4).

Other Promising Features of TRPS. Each individual translocation event (particle passing through the pore) in TRPS generates a trace similar to a peak in analytical chromatography, which has a baseline duration (peak width at the base) and full width half-maxima (fwhm). These parameters are key for understanding particle behavior in suspension and may enable extraction of additional information concerning protein corona thickness on particles, particle charge, and changes in these parameters with time. Particles with higher mobilities (higher particle charge) produce shorter baseline durations whereas particles with lower charge have longer baseline durations. Figure 5 illustrates ENM particle behavior in dispersions obtained in RPMI+FBS and its relationship with particle size. As shown in Figure 5a, SWCNH-ox particles dispersed in 1% FBS display comparatively greater scatter in their fwhm and baseline duration values than the well-stabilized SWCNH-ox particles dispersed in 10% FBS (characterized by a narrow range of fwhm values and a right-skewed baseline duration). The average hydrodynamic diameter ($d_{h,z\text{-ave}}$) of SWCNH-ox particle in 1% FBS was about 50 nm larger than in 10% FBS (Figure 5c). Combined with data in Figure 5a, the TRPS traces reflect the dynamic nature of the dispersion; SWCNH-ox in 1% FBS appear to be poorly stabilized due to insufficient serum in the media, resulting in a mix of particles with variable amounts of serum components coating their surfaces and potentially indicating partial coverage. SWCNH-ox particles are H_2O_2 treated and have carboxylic acid (COOH) and hydroxyl (OH) surface groups (confirmed *via* X-ray photoelectron spectroscopy and fourier transform infrared spectroscopy, data omitted) resulting in a higher net negative surface charge (DLS zeta potential -29.7 ± 0.2 mV in DI water). Upon coating with serum, this negative charge decreases (DLS zeta potential = -9.3 ± 1.0 mV), affecting the mobility of particles in dispersion. Even though SWCNH-ox particles in 1% FBS possess a larger average size, they still remain mobile in the system, as seen from the relatively small baseline durations and fwhm maxima. On the other hand SWCNH-ox particles with 10% FBS have slightly higher baseline durations and much higher fwhm durations. It is interesting to see how these two parameters

change for the other three ENMs under well-dispersed and stabilized dispersion conditions (RPMI +10% FBS). Baseline durations for all ENMs range from 1 to 21 ms (Figure 5b), with the majority of translocation events exhibiting durations in the 1−5 ms range. Higher baseline duration values appear to reflect larger particles and agglomerates, a common observation for ENMs dispersed in serum containing medium.

In contrast with the three other ENMs, which share a similar distribution of baseline duration and fwhm values, a unique pattern was revealed for the Printex 90 particles. In particular, the fwhm values of Printex 90 were significantly larger for translocation times in the range of 0.25−1.5 ms. Printex 90 particles are hydrophobic and form aggregates that are not as uniform in shape and structure as those of the three other ENMs. The TEM images in Figure 1 reveal that, unlike SWCNH-ox, CeO_2 and Ni Inco, which form regular, roughly spherical agglomerates, Printex 90 agglomerates are irregular. These findings reveal that TRPS data holds additional information concerning the shape and mobility of nanoparticles and nanoparticle agglomerates. To the best of our knowledge, no other real-time *in situ* technique can provide such detailed information. Further research in this regard is clearly warranted.

CONCLUSIONS

We have shown that the particle-by-particle analysis by the TRPS technology offers great sensitivity and resolution for the characterization of nanoparticle dispersions in complex biological media compared to the standard DLS technique, which can be greatly beneficial for several applications in nanotoxicology and nanomedicine. Direct measurement of the number concentration for dilute dispersions in small volumes of 50 μL is particularly worthwhile emphasizing. While DLS is a suitable initial characterization technique in such applications and will continue to be widely used, TRPS should be considered as a complementary measurement, and whenever possible, as a primary characterization technique for ENM dispersions. TRPS offers competitive instrumental costs, improved portability and accuracy, and the potential for extracting additional information on aggregate morphology, particle−particle and particle−biomolecule interactions. For all of these reasons, the technique deserves further exploration by the nanotoxicology and nanomedicine community.

MATERIALS AND METHODS

Four distinct ENMs with diverse physicochemical properties were chosen for this work. As detailed in Table 1, H_2O_2 oxidized single wall carbon nanohorns (SWCNH-ox) and Printex 90 are two carbon based nanomaterials, CeO_2 is a metal oxide, and Ni Inco is a nickel nanoparticle developed for catalytic applications (Inconel). Material characterization in the dry phase has been reported previously (refer to Table 1) and included specific surface area by BET, phase identification by XRD, and primary particle size by TEM. Additional chemical characterization included a panel of total and water-soluble metals by inductively coupled plasma mass spectrometry (ICP-MS) and organic and elemental carbon. In addition, each of these materials is characterized for their ability to induce oxidative stress using the serum based ferric reducing ability of serum assay (FRAS), and reported in previous work by us.[48] Ni Inco (Rochester, NY), a high surface area Ni powder developed for catalytic applications, was produced *via* carbonyl-based chemical vapor deposition technology and was partially surface oxidized. ICP-MS analysis yielded 69% Ni, 0.5% Mn, <0.01% Fe, and 1−20 ppm of other elements. Water-soluble Ni was 4%.

ENM Dispersion Protocol. For each ENM dispersion, an optimized dispersion protocol was used.[11] Briefly, a stock ENM solution of 5 mg/mL was prepared by sonicating the ENM powder in DI H_2O for a predetermined time corresponding to the material-specific DSE_{cr} (Table 1). The stock solution was then diluted to 0.5 mg/mL in premixed RPMI + 10% FBS media and stirred (at 800 rpm) at room temperature on a magnetic stir plate for a minimum of 2 h. This protocol yielded reproducible dispersions of good quality, characterized by the smallest achievable $d_{h,z\text{-}ave}$, reasonably small PdI, and good stability. ENM dispersions were then further diluted to the desired concentrations (0.5−50 μg/mL) in cell culture media (RPMI+10% FBS). Dispersions at different concentrations (as specified) were analyzed by DLS, TEM and TRPS.

Dynamic Light Scattering (DLS). ENM dispersion efficiencies under each set of dispersions condition were measured in triplicate by taking intensity-weighted particle size measurements using a dynamic light scattering instrument (Malvern Zetasizer Nano-ZS). The Zetasizer uses a monochromatic coherent 4 mW Helium Neon laser (λ = 633 nm) with a 173° scattering angle and backscatter technology for better sensitivity. The measurements are reported as the z-average hydrodynamic diameter ($d_{h,z\text{-}ave}$) and the software generated particle size polydispersity index (PdI), which is a measure of the width of the particle size distribution. The PdI index is defined as the square of the ratio of standard deviation over the mean particle diameter, PdI = $(\sigma/d)^2$, and calculated automatically by the instrument software. A PdI of <0.1 is considered typically monodisperse distribution,[49] whereas PdI values >0.5−1 indicate polydisperse (polymodal) distributions.[7] The electrophoretic cell was washed with distilled and deionized water to prevent cross contamination. The lab temperature was kept constant at 22 ± 2.5 °C. In brief, during DLS measurements the particles are subjected to Brownian motion. This is compensated by normalization of the electric field autocorrelation function, of which the cumulative analysis is used to obtain the z-average hydrodynamic diameter. "The autocorrelation function is calculated by the Stokes−Einstein equation with the diffusion coefficient determined from the decay time of the autocorrelation function. The scattered light intensity of a particle is proportional to the diameter to the sixth power." Therefore, light scattered by large particles can swamp that of smaller particles and larger particles tend to dominate the scattering characteristics of polydisperse mixtures. For this reason, the change of $d_{h,z\text{-}ave}$ as a function of ultrasonication treatment time only reflects a trend in the change of particle size.[50] The software reports summary statistics of $d_{h,z\text{-}ave}$, PdI and zeta potential (surface charge).

Tunable Resistive Pulse Sensing (TRPS). TRPS size distribution measurements were obtained using a qNano Viro instrument (Izon Science) with NP100-NP400 (40−400 nm size range) and NP400-NP2000 (400−2000 nm) tunable nanopore membranes to cover the entire measurement range of interest. A membrane was attached to a cruciform mount on the instrument, and the electrolyte (RPMI+10% FBS) added into the lower cell (75 μL) and upper cell (45 μL) chambers. All four arms of the cruciform mount were mechanically stretched in the XY axis to ~47 mm

and the pore was allowed to wet with electrolytes. The aperture size was tuned by adjusting the XY deformation in order to optimize the resolution of each ENM preparation. Apertures were calibrated with carboxylated polystyrene nanoparticles (200 nm) supplied by the manufacturer. For all ENM experiments, 45 μL of ENM suspension was added to the upper fluid cell compartment, while the lower cell contained pure RPMI+10% FBS solution. Experimental conditions such as the degree of membrane stretch (the means of pore size adjustment) and applied voltage were tuned to optimize the resolution for each ENM preparation. Pressure was applied to the top fluid cell as determined by the water-based variable pressure module (IZON Science), and varied by 500 Pa at 30 s increments. The range of pressures applied was from 300 Pa to −600 Pa (vacuum). A minimum of 500 translocation events were recorded for each sample. The instrument provided software was used to calculate particle size distribution statistics. The raw data from DLS and TRPS were exported and further analyzed and plotted using Origin 8.0 software. From the TRPS data, we further calculated typical summary statistics of log-normal distributions, including the arithmetic mean (AM), geometric mean (GM), and geometric standard deviation of the size distributions. Following investigation of the cumulative probability plots, and the formal test for log-normality of size distribution with Shapiro-Wilks (W-) statistics, it was concluded that the TRPS size distributions were log-normal (W-test, $p > 0.05$ in all cases). The fraction of particle number for each peak size range was calculated from the total number.

Transmission Electron Microscopy (TEM). The particle size and morphology of ENMs dispersed in cell culture media were evaluated using transmission electron microscopy on a Philips EM 400T microscope. The ENM samples were diluted to 50 μg/mL in DI water from a stock dispersion of 0.5 mg/mL. The TEM samples were then prepared by drop casting ENM dispersions on TEM grids. The grids were allowed to air-dry before imaging.

Cell Culture and ENM Dosing. We used a phorbol myristate acetate (PMA, Sigma-Aldrich) induced human monocyte/macrophage (THP-1) leukemia cell line for this study. Cells were maintained in RPMI 1640 medium containing 10% heat-inactivated FBS and supplemented with penicillin G (50 U/mL) and streptomycin sulfate (50 μg/mL). Cells were grown and maintained in 75 cm^2 cell culture flasks (Corning) at 37 °C in 5% CO_2 in a humidified incubator. When confluent, THP-1 cells were centrifuged and seeded in 96-well plates (VWR Scientific) at 5×10^5 cells/mL (total volume 200 μL/well), in the presence of 20 ng/mL (MA, Sigma-Aldrich) in order to differentiate them into mature macrophage-like cells. Twenty-four hours after seeding, 100 μL of the medium was removed, and cells were treated with different ENM doses in the 1−50 μg/mL range (0, 1, 5, 10, 30, 50) or an equivalent amount of medium alone.

For the purposes of this paper, which were to investigate the impact of differences in particle size distribution measurements and dosimetry estimates on cytotoxicity end points, we used cell viability (MTT) data.

MTT Assay. Cell viability was determined using an MTT kit from the American Type Culture Collection (ATCC, VA). In brief, the yellow tetrazolium MTT (3-(4, 5-dimethylthiazolyl-2)-2, 5-diphenyltetrazolium bromide) is reduced to purple formazan by metabolically active cells, in part by the action of dehydrogenase enzymes. The resulting intracellular purple formazan can be solubilized using detergent and quantified spectrophotometrically by measuring absorbance at 570 nm. After the appropriate ENM dosing time (6 or 24 h), 200 μL of supernatant was removed and cells were washed twice with PBS. Per ATCC protocol, cells were then incubated with 10 μL of the MTT reagent followed with 90 μL of fresh medium. Cells were further incubated for 2 to 4 h until a purple precipitate was visible. Once crystals were observed in the wells, the supernatant with MTT reagent was removed and 100 μL of detergent reagent was added. The plate was left at room temperature in the dark for 2 h and absorbance was recorded at 570 nm. Percent viability was calculated relative to controls (undosed cells). H_2O_2 was used as positive control.

Dose Calculations. *Effective Density Determination.* Effective density of all ENM samples was determined by using a volumetric centrifugation protocol.[51] Briefly, 50 μg/mL of an ENM suspension was aliquoted into a TPP packed cell volume (PCV) tube (Techno Plastic Products, Trasadingen, Switzerland) and centrifuged at 1000*g* for 1 h to form a pellet containing all of the ENM plus any bound serum components. The pellet volume was measured using a slide rule-like easy-measure device also obtained from the PCV tube manufacturer. Effective density was then calculated from the pellet volumes of each ENM as described by Cohen *et al.*[51]

Calculation of Deposited Fraction. A recently developed integrated dispersion and dosimetry platform at Harvard[52] was used to calculate the fraction of administered ENM particles that would be deposited onto cells as a function of time, $f_D(t)$. The particle hydrodynamic diameter, $d_{h,z\text{-}ave}$, as measured by TRPS, and effective density (Table 1) were used as ISDD model inputs, in addition to the following parameters: media column height, 3.3 mm; temperature, 310 K; media density, 1.00 g/mL; viscosity, 0.00074 Pa × s for RPMI/10% FBS[52] and administered (initial suspension) particle concentration, 50 μg/mL.

Since TRPS resulted in two peaks (one similar to the DLS peak and another corresponding to significantly larger particle agglomerates), each peak was fitted separately using the model. The effective density of the large particle fraction could not be measured experimentally and was assumed to be equal to that of smaller agglomerates. reported in Table 1. Because large agglomerates may trap a higher volume of liquid media in-between particles, their effective density may be slightly lower than of smaller agglomerates. We have addressed the associated uncertainties of this assumption *via* sensitivity analysis. If effective densities of larger agglomerates were to be higher that values in Table 1, then these larger agglomerates would settle much faster than predicted. If large agglomerates were to have lower effective densities than of the smaller agglomerates, then overestimation of the *f*(D) function would occur. On the basis of sensitivity analysis using lower effective densities values down to 1.1 (g/mol), the impact of this assumption on the overall TRPS deposition curve was <5%.

For each ENM-media combination, the model derived $f_D(t)$ was fit to a Gompertz sigmoidal equation as follows:

$$f_D(t) = 1 - e^{-at} \quad (1)$$

where t is time (h) and a is a particle- and media-specific deposition fraction constant (h^{-1}). The deposition fraction constant a (h^{-1}) was calculated for each ENM-media combination.

Solving eq 1 for the time t at which the fraction $f_D(t)$ of administered particles is delivered yields

$$t = -\ln(1 - f_D(t))/a \quad (2)$$

eq 2 was used to calculate the time required for the delivery of 50% of the administered dose, t_{50}, for each ENM-media combination using the specific deposition function constant a and an $f_D(t_{50})$ value of 0.50. The same approach was used to calculate the time required for the delivery of 90% of the administered dose (t_{90}).

For the TRPS-based modeling, two separate $f_D(t)$ functions were used to calculate the overall deposited dose to cells based on the relative concentration of each population at each time point using the following formula:

$f_D(t)$ TRPS = fractional area of first mode × $f_D(t)$ of first mode + fractional area of second mode × $f_D(t)$ second mode. For example, for SWCNH-ox at 24 h (data in Table 2 and Figure 3), the resultant $f_D(t)$ TRPS = 0.84 × 0.19 + 0.16 × 0.27 = 0.16 + 0.04 = 0.20. Results of these calculations for 6 and 24 h time point are summarized in Table 4.

In Vitro Dose−Response Relationships. Slopes of dose−response relationships were derived from fitted regression lines on the cell viability-nanoparticle mass dose data. Three doses were used, resulting in three slopes: administered dose, delivered dose using hydrodynamic particle size input from DLS, and delivered dose calculates as above from TRPS size distributions. The impact of size distribution measurements on dosimetry and dose−response relationship s was investigated by looking at changes in the slopes (ratios of slopes), as well as relative differences (slope TRPS − slope DLS)/slope DLS), as described in the footnote on Figure 4.

Conflict of Interest: The authors declare no competing financial interest.

Acknowledgment. The study was supported by Nanoscale Science and Engineering Centers Program of the National Science Foundation #0425826 and EEC-0425826 (Supplement), National Science Foundation (Grant No. 1235806) and NIH (Grant No. P30ES000002). The authors would like to acknowledge Joel Cohen from HSPH for his help with the dose calculations.

REFERENCES AND NOTES

1. Luyts, K.; Napierska, D.; Nemery, B.; Hoet, P. H. M. How Physico-chemical Characteristics of Nanoparticles Cause their Toxicity: Complex and Unresolved Interrelations. *Environ. Sci.: Processes Impacts* **2013**, *15*, 23–38.
2. Oberdorster, G.; Maynard, A.; Donaldson, K.; Castranova, V.; Fitzpatrick, J.; Ausman, K.; Carter, J.; Karn, B.; Kreyling, W.; Lai, D.; *et al.* Principles for Characterizing the Potential Human Health Effects from Exposure to Nanomaterials: Elements of a Screening Strategy. *Part. Fibre Toxicol.* **2005**, *2*, 8.
3. Nel, A.; Mädler, L.; Velegol, D.; Xia, T.; Hoek, E.; Somasundaran, P.; Klaessig, F.; Castranova, V.; Thompson, M. Understanding Biophysicochemical Interactions at the Nano-bio Interface. *Nat. Mater.* **2009**, *8*, 543–557.
4. Shvedova, A. A.; Kagan, V. E.; Fadeel, B. Close Encounters of the Small Kind: Adverse Effects of Man-made Materials Interfacing with the Nano-cosmos of Biological Systems. *Annu. Rev. Pharmacol. Toxicol.* **2010**, *50*, 63–88.
5. Borm, P. J.; Robbins, D.; Haubold, S.; Kuhlbusch, T.; Fissan, H.; Donaldson, K.; Schins, R.; Stone, V.; Kreyling, W.; Lademann, J.; *et al.* The Potential Risks of Nanomaterials: a Review Carried Out for ECETOC. *Part. Fibre Toxicol.* **2006**, *3*, 11.
6. Dobrovolskaia, M. A.; McNeil, S. E. Immunological Properties of Engineered Nanomaterials. *Nat. Nanotechnol.* **2007**, *2*, 469–478.
7. Bihari, P.; Vippola, M.; Schultes, S.; Praetner, M.; Khandoga, A. G.; Reichel, C. A.; Coester, C.; Tuomi, T.; Rehberg, M.; Krombach, F. Optimized Dispersion of Nanoparticles for Biological *In Vitro* and *In Vivo* Studies. *Part. Fibre Toxicol.* **2008**, *5*, 14.
8. Taurozzi, J. S.; Hackley, V. A.; Wiesner, M. R. Ultrasonic Dispersion of Nanoparticles for Environmental, Health and Safety Assessment-Issues and Recommendations. *Nanotoxicology* **2011**, *5*, 711–729.
9. Boverhof, D. R.; David, R. M. Nanomaterial Characterization: Considerations and Needs for Hazard Assessment and Safety Evaluation. *Anal. Bioanal. Chem.* **2010**, *396*, 953–961.
10. Warheit, D. How Meaningful Are the Results of Nanotoxicity Studies in the Absence of Adequate Material Characterization? *Toxicol. Sci.* **2008**, *101*, 183–185.
11. Cohen, J.; Deloid, G.; Pyrgiotakis, G.; Demokritou, P. Interactions of Engineered Nanomaterials in Physiological Media and Implications for *In Vitro* Dosimetry. *Nanotoxicology* **2013**, *7*, 417–431.
12. DeLoid, G.; Cohen, J. M.; Darrah, T.; Derk, R.; Rojanasakul, L.; Pyrgiotakis, G.; Wohlleben, W.; Demokritou, P. Estimating the Effective Density of Engineered Nanomaterials for *In Vitro* Dosimetry. *Nat. Commun.* **2014**, *5*, 3514.
13. Cohen, J. M.; Teeguarden, J. G.; Demokritou, P. An Integrated Approach for the *In Vitro* Dosimetry of Engineered Nanomaterials. *Part. Fibre Toxicol.* **2014**, *11*, 20.
14. Cohen, J. M.; Derk, R.; Wang, L.; Godleski, J.; Kobzik, L.; Brain, J.; Demokritou, P. Tracking Translocation of Industrially Relevant Engineered Nanomaterials (ENMs) Across Alveolar Epithelial Monolayers *In Vitro*. *Nanotoxicology* **2014**, *0*, 1–10.
15. Pyrgiotakis, G.; Blattmann, C. O.; Pratsinis, S.; Demokritou, P. Nanoparticle-Nanoparticle Interactions in Biological Media by Atomic Force Microscopy. *Langmuir* **2013**, *29*, 11385–11395.
16. Pyrgiotakis, G.; Blattmann, C. O.; Demokritou, P. Real-Time Nanoparticle–Cell Interactions in Physiological Media by Atomic Force Microscopy. *ACS Sustainable Chem. Eng.* **2014**, *2*, 1681–1690.
17. Crist, R. M.; Grossman, J. H.; Patri, A. K.; Stern, S. T.; Dobrovolskaia, M. A.; Adiseshaiah, P. P.; Clogston, J. D.; McNeil, S. E. Common Pitfalls in Nanotechnology: Lessons Learned from NCI's Nanotechnology Characterization Laboratory. *Integr. Biol.* **2013**, *5*, 66–73.
18. Albanese, A.; Tang, P. S.; Chan, W. C. The Effect of Nanoparticle Size, Shape, and Surface Chemistry on Biological Systems. *Annu. Rev. Biomed. Eng.* **2012**, *14*, 1–16.
19. Champion, J. A.; Mitragotri, S. Role of Target Geometry in Phagocytosis. *Proc. Natl. Acad. Sci. U. S. A.* **2006**, *103*, 4930–4934.
20. Ji, Z.; Jin, X.; George, S.; Xia, T.; Meng, H.; Wang, X.; Suarez, E.; Zhang, H.; Hoek, E. M.; Godwin, H.; *et al.* Dispersion and Stability Optimization of TiO_2 Nanoparticles in Cell Culture Media. *Environ. Sci. Technol.* **2010**, *44*, 7309–7314.
21. Walczyk, D.; Bombelli, F. B.; Monopoli, M. P.; Lynch, I.; Dawson, K. A. What the Cell "Sees" in Bionanoscience. *J. Am. Chem. Soc.* **2010**, *132*, 5761–5768.
22. Demokritou, P.; Gass, S.; Pyrgiotakis, G.; Cohen, J. M.; Goldsmith, W.; McKinney, W.; Frazer, D.; Ma, J.; Schwegler-Berry, D.; Brain, J.; *et al.* An *In Vivo* and *In Vitro* Toxicological Characterisation of Realistic Nanoscale CeO(2) Inhalation Exposures. *Nanotoxicology* **2013**, *7*, 1338–1350.
23. Khatri, M.; Bello, D.; Pal, A. K.; Cohen, J. M.; Woskie, S.; Gassert, T.; Lan, J.; Gu, A. Z.; Demokritou, P.; Gaines, P. Evaluation of Cytotoxic, Genotoxic and Inflammatory Responses of Nanoparticles from Photocopiers in Three Human Cell Lines. *Part. Fibre Toxicol.* **2013**, *10*, 42.
24. Oberdorster, G.; Oberdorster, E.; Oberdorster, J. Nanotoxicology: an Emerging Discipline Evolving from Studies of Ultrafine Particles. *Environ. Health Perspect.* **2005**, *113*, 823–839.
25. Thomas, K.; Sayre, P. Research Strategies for Safety Evaluation of Nanomaterials, Part I: Evaluating the Human Health Implications of Exposure to Nanoscale Materials. *Toxicol. Sci.* **2005**, *87*, 316–321.
26. Powers, K. W.; Palazuelos, M.; Moudgil, B. M.; Roberts, S. M. Characterization of the Size, Shape, and State of Dispersion of Nanoparticles for Toxicological Studies. *Nanotoxicology* **2007**, *1*, 42–51.
27. Luykx, D. M.; Peters, R. J.; van Ruth, S. M.; Bouwmeester, H. A Review of Analytical Methods for the Identification and Characterization of Nano Delivery Systems in Food. *J. Agric. Food Chem.* **2008**, *56*, 8231–8247.
28. Montes-Burgos, I.; Walczyk, D.; Hole, P.; Smith, J.; Lynch, I.; Dawson, K. Characterisation of Nanoparticle Size and State Prior to Nanotoxicological Studies. *J. Nanopart. Res.* **2010**, *12*, 47–53.
29. Dobrovolskaia, M. A.; Patri, A. K.; Zheng, J.; Clogston, J. D.; Ayub, N.; Aggarwal, P.; Neun, B. W.; Hall, J. B.; McNeil, S. E. Interaction of Colloidal Gold Nanoparticles with Human Blood: Effects on Particle Size and Analysis of Plasma Protein Binding Profiles. *Nanomedicine* **2009**, *5*, 106–117.
30. Taurozzi, J. S.; Hackley, V. A.; Wiesner, M. R. A Standardised Approach for the Dispersion of Titanium Dioxide Nanoparticles in Biological Media. *Nanotoxicology* **2013**, *7*, 389–401.
31. Powers, K. W.; Brown, S. C.; Krishna, V. B.; Wasdo, S. C.; Moudgil, B. M.; Roberts, S. M. Research Strategies for Safety Evaluation of Nanomaterials. Part VI. Characterization of Nanoscale Particles for Toxicological Evaluation. *Toxicol. Sci.* **2006**, *90*, 296–303.
32. Merkus, H. G. *Particle Size Measurements: Fundamentals, Practice, Quality*; Springer: Berlin, 2008.
33. Kozak, D.; Anderson, W.; Vogel, R.; Chen, S.; Antaw, F.; Trau, M. Simultaneous Size and Zeta-potential Measurements of Individual Nanoparticles in Dispersion Using Size-tunable Pore Sensors. *ACS Nano* **2012**, *6*, 6990–6997.
34. Anderson, W.; Kozak, D.; Coleman, V. A.; Jamting, A. K.; Trau, M. A Comparative Study of Submicron Particle Sizing

Platforms: Accuracy, Precision and Resolution Analysis of Polydisperse Particle Size Distributions. *J. Colloid Interface Sci.* **2013**, *405*, 322–330.
35. Murdock, R. C.; Braydich-Stolle, L.; Schrand, A. M.; Schlager, J. J.; Hussain, S. M. Characterization of Nanomaterial Dispersion in Solution Prior to in vitro Exposure Using Dynamic Light Scattering Technique. *Toxicol. Sci.* **2008**, *101*, 239–253.
36. DeBlois, R. W.; Bean, C. P.; Wesley, R. K. A. Electrokinetic Measurements with Submicron Particles and Pores by the Resistive Pulse Technique. *J. Colloid Interface Sci.* **1977**, *61*, 323–335.
37. Ito, T.; Sun, L.; Bevan, M. A.; Crooks, R. M. Comparison of Nanoparticle Size and Electrophoretic Mobility Measurements Using a Carbon-Nanotube-Based Coulter Counter, Dynamic Light Scattering, Transmission Electron Microscopy, and Phase Analysis Light Scattering. *Langmuir* **2004**, *20*, 6940–6945.
38. Ito, T.; Sun, L.; Crooks, R. M. Simultaneous Determination of the Size and Surface Charge of Individual Nanoparticles Using a Carbon Nanotube-Based Coulter Counter. *Anal. Chem.* **2003**, *75*, 2399–2406.
39. Berge, L. I.; Feder, J.; Jossang, T. A Novel Method to Study Single-particle Dynamics by the Resistive Pulse Technique. *Rev. Sci. Instrum.* **1989**, *60*, 2756–2763.
40. Platt, M.; Willmott, G. R.; Lee, G. U. Resistive Pulse Sensing of Analyte-induced Multicomponent Rod Aggregation Using Tunable Pores. *Small* **2012**, *8*, 2436–2444.
41. Golibersuch, D. C. Observation of Aspherical Particle Rotation in Poiseuille Flow *via* the Resistance Pulse Technique. I. Application to Human Erythrocytes. *Biophys. J.* **1973**, *13*, 265–280.
42. Holden, D. A.; Hendrickson, G.; Lyon, L. A.; White, H. S. Resistive Pulse Analysis of Microgel Deformation During Nanopore Translocation. *J. Phys. Chem. C* **2011**, *115*, 2999–3004.
43. Kozak, D.; Anderson, W.; Grevett, M.; Trau, M. Modeling Elastic Pore Sensors for Quantitative Single Particle Sizing. *J. Phys. Chem. C* **2012**, *116*, 8554–8561.
44. Pal, A. K.; Bello, D.; Budhlall, B.; Rogers, E.; Milton, D. K. Screening for Oxidative Stress Elicited by Engineered Nanomaterials: Evaluation of Acellular DCFH Assay. *Dose-Response* **2012**, *10*, 308–330.
45. Horie, M.; Nishio, K.; Fujita, K.; Endoh, S.; Miyauchi, A.; Saito, Y.; Iwahashi, H.; Yamamoto, K.; Murayama, H.; Nakano, H.; *et al.* Protein Adsorption of Ultrafine Metal Oxide and its Influence on Cytotoxicity Toward Cultured Cells. *Chem. Res. Toxicol.* **2009**, *22*, 543–553.
46. Lin, S.; Zhao, Y.; Xia, T.; Meng, H.; Ji, Z.; Liu, R.; George, S.; Xiong, S.; Wang, X.; Zhang, H.; *et al.* High Content Screening in Zebrafish Speeds up Hazard Ranking of Transition Metal Oxide Nanoparticles. *ACS Nano* **2011**, *5*, 7284–7295.
47. Lim, C. H.; Kang, M.; Han, J. H.; Yang, J. S. Effect of Agglomeration on the Toxicity of Nano-sized Carbon Black in Sprague-Dawley Rats. *Environ. Health Toxicol.* **2012**, *27*, e2012015.
48. Hsieh, S. F.; Bello, D.; Schmidt, D. F.; Pal, A. K.; Stella, A.; Isaacs, J. A.; Rogers, E. J. Mapping the Biological Oxidative Damage of Engineered Nanomaterials. *Small* **2013**, *9*, 1853–1865.
49. Camli, S. T.; Buyukserin, F.; Balci, O.; Budak, G. G. Size Controlled Synthesis of Sub-100 nm Monodisperse Poly(methylmethacrylate) Nanoparticles Using Surfactant-Free Emulsion Polymerization. *J. Colloid Interface Sci.* **2010**, *344*, 528–532.
50. Krause, B.; Mende, M.; Pötschke, P.; Petzold, G. Dispersability and Particle Size Distribution of CNTs in an Aqueous Surfactant Dispersion as a Function of Ultrasonic Treatment Time. *Carbon* **2010**, *48*, 2746–2754.
51. Demokritou, P.; DeLoid, G.; Cohen, J. Novel Methods of Measuring Effective Density of Nanoparticles in Fluids. WO/2013/192412, June 20, 2012.
52. Hinderliter, P. M.; Minard, K. R.; Orr, G.; Chrisler, W. B.; Thrall, B. D.; Pounds, J. G.; Teeguarden, J. G. ISDD: A Computational Model of Particle Sedimentation, Diffusion and Target Cell Dosimetry for *In Vitro* Toxicity Studies. *Part. Fibre Toxicol.* **2010**, *7*, 36.